Composites Part B 126 (2017) 60–71

Contents lists available at ScienceDirect

Composites Part B

journal homepage: www.elsevier.com/locate/compositesb

Modelling the damage evolution in notched omega stiffened composite panels under compression☆

A. Riccio [a], A. Sellitto [a, *], S. Saputo [a], A. Russo [a], M. Zarrelli [b], V. Lopresto [c]

[a] Department of Industrial and Informatics Engineering, Università degli studi della Campania "Luigi Vanvitelli", via Roma 29, Aversa, CE, Italy
[b] CNR-IPCB Institute for Composites, Polymers and Biomaterials, National Research Council of Italy, P.le E Fermi, Portici, NA, Italy
[c] Department of Material Engineering, University of Naples "FEDERICO II", Pl.e Tecchio, Naples, Italy

ARTICLE INFO

Article history:
Received 23 January 2017
Received in revised form
21 April 2017
Accepted 21 May 2017
Available online 25 May 2017

Keywords:
Intra-laminar damage
Large notch damage
Finite element model
Delamination
Cohesive model

ABSTRACT

In this paper, the compressive behaviour of an omega stiffened composite panel with a large notch damage has been investigated. The influence of intra-laminar and inter-laminar damage onset and evolution on the compressive behaviour of a stiffened panel, characterised by a cut-out located in the middle bay and oriented at 45° with respect to the load direction, has been studied. A numerical model, taking into account delamination and fibre-matrix damage evolution, respectively, by means of cohesive elements and Hashin's failure criteria together with material degradation rules, has been adopted. By comparing the performed numerical analyses, taking into account intra-laminar and inter-laminar damages, the effects of the interaction between delaminations and fibre-matrix damage in the large notch area on the global compressive behaviour of the omega stiffened composite panel have been assessed and critically discussed.

1. Introduction

In the recent years, composite materials have driven scientific and technological developments in several engineering areas. Indeed, the high strength and stiffness, as well as the durability and the versatility, are the main reasons for their employment for structural applications especially in transportation engineering fields. Particularly, in the aerospace field, fibre-reinforced composite materials are even more adopted due to their excellent stiffness-weight ratio if compares to the classical metallic alloys. On the other hand, differently from metal alloys, the composite materials damage mechanisms are complex and difficult to predict and control. Indeed, different damage mechanisms, such as intra-laminar and inter-laminar failures, can arise and interact in composite laminates. These damage mechanisms, which include matrix cracking, fibre breakage, fibre–matrix debonding and delamination, which can be arise as manufacturing defects or due to the applied loads, can lead to a premature structure collapse.

One of the most critical aspects related to composites application for the manufacturing of structural component is their damage behaviour under compressive load [1–6]. Many authors have investigated the buckling and post-buckling performances of aeronautical composite panels. In Ref. [7] the buckling and post-buckling behaviour of aeronautical stiffened composite panels are experimentally and numerically investigated. In Ref. [8] the compressive behaviour of a hat-stringer-stiffened composite flat panel is investigated; experimental and numerical results are presented to assess the buckling and post-buckling responses of the panel. Wang et al. [9] present an experimental and numerical investigation of the post-buckling behaviour of stiffened composite panels with pre-damage. The complexity of the compressive behaviour of composite structures becomes more relevant when the presence of cut-outs is considered [10–13]. In Ref. [14] the effect of cut-out on the buckling and post-buckling behaviour of a carbon/epoxy composite C-section structure is investigated. Diamond and circular cut-outs are considered in the C-section web, causing a slight decrease in the critical buckling load. In Ref. [15] FEM buckling analyses have been performed on composite square plates with elliptical notches. The effects of the notch orientation angle have been analysed.

Whatever is the mechanical load, acting on composite structures, in order to correctly predict their mechanical behaviour,

☆ The results of this work have been presented at the International Symposium on Dynamic Response and Failure of Composite Materials, Draf2016, Ischia, Naples, 6–9 September 2016.

* Corresponding author.
E-mail address: andrea.sellitto@unina2.it (A. Sellitto).

http://dx.doi.org/10.1016/j.compositesb.2017.05.067
1359-8368/

intra-laminar and inter-laminar damages onset and propagation need to be taken into account, respectively, by means of a Progressive Damage Approach (PFA) [16–22] and Virtual Crack Closure Technique (VCCT) or Cohesive interfaces [23,24]. In Ref. [25] a finite element model is created to perform progressive failure analyses on notched composite laminates. In Ref. [26] a progressive damage model is presented for notched laminated composites subjected to tensile loading. Additionally, several works can be found in literature describing the inter-laminar damage models [27–33].

Even if literature presents a wide range of models able to take into account the different failure mechanisms acting in stiffened composite panels, the interaction between these damage mechanisms and their influence on the global mechanical behaviour, strictly related to the geometrical and material configuration of stringers and skin, needs to be further studied both by numerical and experimental investigations.

In this paper, the compressive behaviour of an omega stiffened composite panel with a large notch damage is numerically investigated. The influence of intra-laminar and inter-laminar damage onset and evolution on the compressive behaviour a stiffened panel, characterised by a cut-out located in the middle bay and oriented at 45° with respect to the load direction, has been studied. A numerical model, taking into account delaminations and fibre-matrix damages evolution, respectively, by means of cohesive elements and Hashin's failure criteria together with material degradation rules, has been adopted. Two numerical analyses have been carried out: the first one takes into account only the intra-laminar failure onset and evolution while the second one considers both intra-laminar and inter-laminar damage mechanisms. By comparing the numerical results from these two analyses, the effects of the interaction between delaminations and fibre-matrix damage in the large notch area on the global compressive behaviour of the omega stiffened composite panel have been assessed and critical discussed.

In section 2, the theoretical background behind the damage models used in this work is presented, while in section 3, the geometry of the investigated stiffened panel together with the FEM model and numerical results are introduced. The numerical results in terms of compressive load as a function of the applied displacement, matrix cracking and fibre breakage evolution are presented and compared.

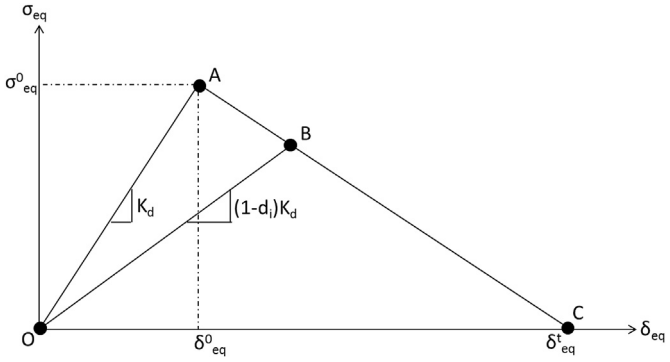

Fig. 1. Constitutive relation.

2. Theoretical background

Composite laminates damage mechanisms can be grouped in two main sets: *intra-laminar* damage mechanisms, arising within each lamina (such as matrix cracking and fibre breakage), and *inter-laminar* damage mechanisms, arising between two adjacent laminae (such as debonding and delaminations). Intra-laminar damage initiation and propagation can be identified by adopting several failure criteria which can be grouped in:

- *Limit criteria*, such as the Maximum stress and the Maximum strain criteria, which can predict the failure according to the magnitude of stress or strain components without consider the interactions among them;
- *Interactive criteria*, such as the Tsai-Wu and the Tsai-Hill criteria, which assume that all the stress components simultaneously contribute to the lamina failure.
- *Separate mode criteria*, such as Hashin's failure criterion, which separate the criterion for matrix failure mode from the criterion for fibre failure mode. The criteria for each failure mode may involve stress interactions.

In this work, intralaminar damages have been investigated by using Hashin's failure criterion. The simulation of the inter-laminar damage onset and propagation can be numerically performed by adopting two main different approaches among others. The first is the *Virtual Crack Closure Technique* (VCCT), which is based on the linear elastic fracture mechanics. An alternative approach, which is the one adopted in the present work, is the one based on the *Cohesive Zone Method* (CZM). In the next subsections, the approaches adopted for the simulation of intra-laminar and inter-laminar damage onset and evolution are briefly described.

2.1. Hashin's failure criteria and material degradation rules

The Hashin's failure criteria allow to check for intra-laminar failure modes. Four different modes of failure can be introduced: tensile fibre failure, compressive fibre failure, tensile matrix failure and compressive matrix failure. The Hashin's formulation, adopted in this paper, is described by Equations (1)–(4), where F_{ft}, F_{fc}, F_{mt}, and F_{mc} are respectively the fibre tensile, fibre compressive, matrix tensile and matrix compressive criterion.

$$F_{ft} = \left(\frac{\widehat{\sigma}_{11}}{X_T}\right)^2 + \left(\frac{\widehat{\sigma}_{12}}{S_L}\right)^2 = 1 \tag{1}$$

Table 1
Equivalent displacement and stress definition.

	Fibre tension	Fibre compression	Matrix tension	Matrix compression
δ_{eq}	$L_c\sqrt{\langle\varepsilon_{11}\rangle^2+\varepsilon_{12}^2}$	$L_c\langle-\varepsilon_{11}\rangle$	$L_c\sqrt{\langle\varepsilon_{22}\rangle^2+\varepsilon_{12}^2}$	$L_c\sqrt{\langle-\varepsilon_{22}\rangle^2+\varepsilon_{12}^2}$
σ_{eq}	$\frac{L_c(\langle\sigma_{11}\rangle\langle\varepsilon_{11}\rangle+\sigma_{12}\cdot\varepsilon_{12})}{\delta_{ft,eq}}$	$\frac{L_c\langle-\sigma_{11}\rangle\langle-\varepsilon_{11}\rangle}{\delta_{fc,eq}}$	$\frac{L_c(\langle\sigma_{22}\rangle\langle\varepsilon_{22}\rangle+\sigma_{12}\cdot\varepsilon_{12})}{\delta_{mt,eq}}$	$\frac{L_c(\langle-\sigma_{22}\rangle\langle-\varepsilon_{22}\rangle+\sigma_{12}\cdot\varepsilon_{12})}{\delta_{mc,eq}}$

$$F_{fc} = \left(\frac{\widehat{\sigma}_{11}}{X_C}\right)^2 = 1 \tag{2}$$

$$F_{mt} = \left(\frac{\widehat{\sigma}_{22}}{Y_T}\right)^2 + \left(\frac{\widehat{\sigma}_{12}}{S_L}\right)^2 = 1 \tag{3}$$

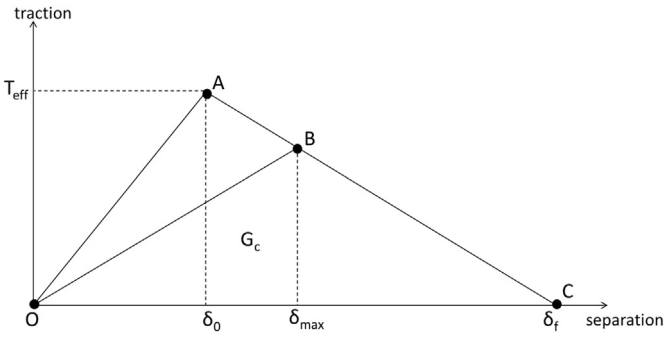

Fig. 2. Traction-separation law for cohesive material.

$$F_{mc} = \left(\frac{\widehat{\sigma}_{22}}{2S_T}\right)^2 + \left[\left(\frac{Y_C}{2S_T}\right)^2 - 1\right]\cdot\frac{\widehat{\sigma}_{22}}{Y_C} + \left(\frac{\widehat{\sigma}_{12}}{S_L}\right)^2 = 1 \tag{4}$$

According to Equations (1)–(4), $\widehat{\sigma}_{11}$ and $\widehat{\sigma}_{22}$ are respectively the stress in the fibre direction and normal to the fibre direction; X_T, X_C, Y_T, Y_C, S_L, and S_T are respectively the fibre tensile, fibre compressive, matrix tensile, matrix compressive, longitudinal and transversal shear strengths.

The constitutive relation adopted for each failure mode evolution to represent the material degradation is illustrated in Fig. 1.

According to Fig. 1, the segment OA identifies the undamaged material phase, with initial stiffness K_d. The segment AC identifies the material degradation phase. Indeed, along the segment AC (the point A actually represents the Hashin's stress limit value) the material stiffness K is reduced according to Equation (5).

$$K = (1 - \mathrm{d_i})\cdot K_d \tag{5}$$

The parameter d_i is the degradation coefficient described by Equation (6).

$$d_i = \frac{\delta^t_{i,eq}\left(\delta_{i,eq} - \delta^0_{i,eq}\right)}{\delta_{i,eq}\left(\delta^t_{i,eq} - \delta^0_{i,eq}\right)}; \quad \delta^0_{i,eq} \le \delta_{i,eq} \le \delta^t_{i,eq}; \quad i \in (f_c, f_t, m_c, m_t) \tag{6}$$

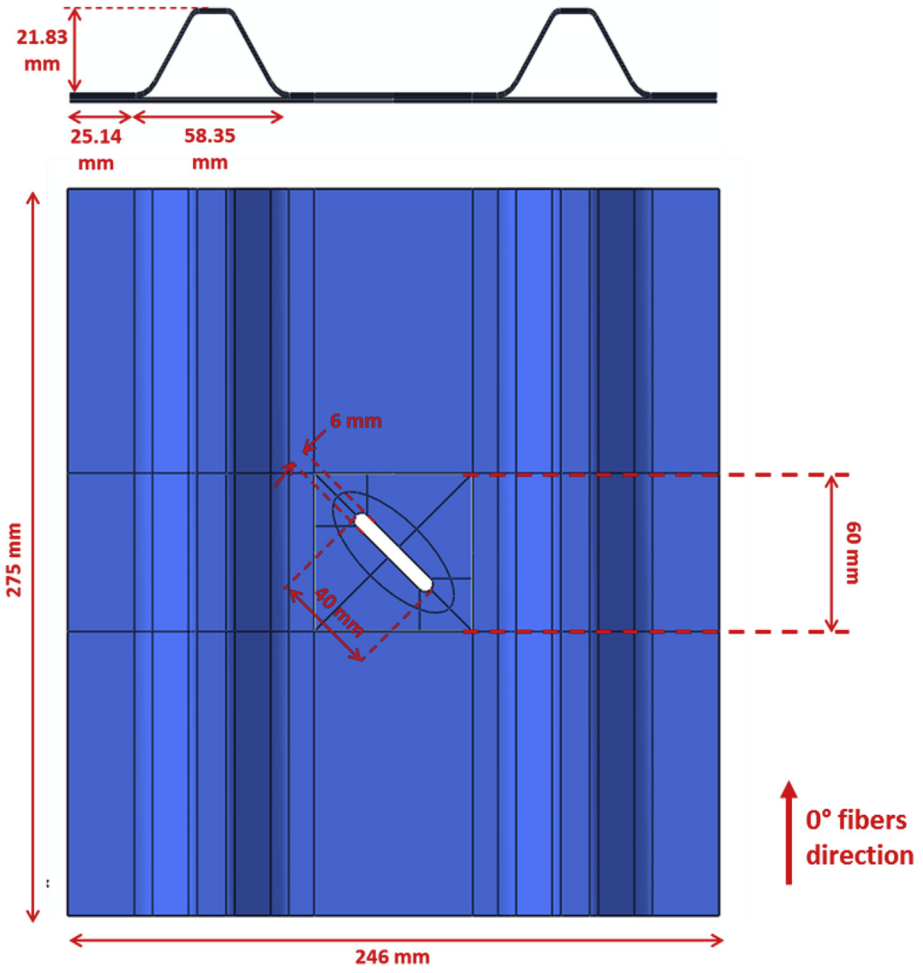

Fig. 3. Geometrical description of the specimen.

Table 2
Orthotropic properties of the adopted material system.

Properties	Value
E_{11}	130050 MPa
E_{22}	11550 MPa
G_{12}	6000 MPa
G_{13}	6000 MPa
G_{23}	6000 MPa
ν_{12}	0.312
ν_{13}	0.312
ν_{23}	0.312
G_{Ic}	0.18 kJ/m^2
$G_{IIc} = G_{IIIc}$	0.5 kJ/m^2

Table 3
Intra-laminar strengths.

Properties	Value
X_T	1022 MPa
X_C	614 MPa
Y_C	54 MPa
Y_T	169 MPa
S_T	63 MPa
S_C	28 MPa
G^T_{Ic}	11.5 kJ/m^2
G^C_{Ic}	4.1 kJ/m^2
G^T_{IIc}	0.35 kJ/m^2
G^C_{IIc}	3.2 kJ/m^2

The equivalent displacement $\delta^t_{i,eq}$, identifying the completely damaged material (point C in Fig. 1), can be calculated by using Equation (7).

$$\delta^t_{i,eq} = \frac{2G_c}{\sigma^0_{i,eq}} \tag{7}$$

where G_c represents the fracture energy and $\sigma^0_{i,eq}$ is the equivalent stress at which the Hashin's criterion is satisfied.

The equivalent displacements and stresses, as a function of stress and strain components, for each failure mode are described in Table 1.

According to Table 1, L_c is the element characteristic length which can be assumed equal to the element edge, while < > is the Macauley bracket operator defined by Equation (8).

$$\langle \gamma \rangle = \frac{\gamma + |\gamma|}{2} \quad \forall \gamma \in \Re \tag{8}$$

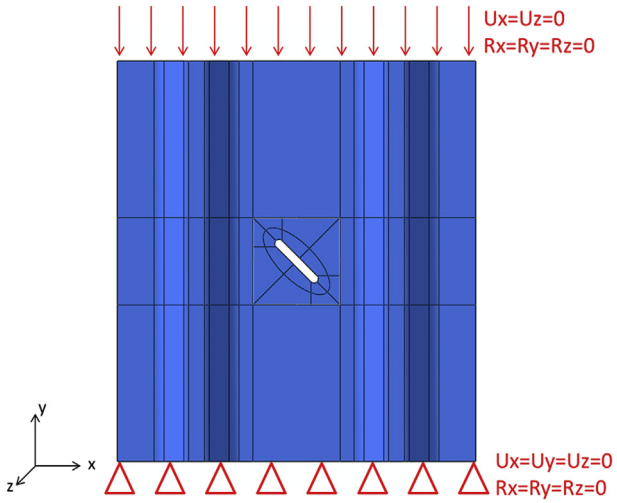

Fig. 5. Boundary conditions.

2.2. Cohesive zone model

Cohesive elements have been used to numerically simulate the interlaminar damage onset and propagation. The considered cohesive constitutive response, schematically shown in Fig. 2, is based on two different phases: the initial damage phase, which is representative of the damage onset, and the evolution damage phase, representative of the damage propagation.

The Quadratic Nominal Stress Criterion (QUADS) has been used for the evaluation of the damage onset (point A in Fig. 2) taking into account the presence of mixed mode delamination propagation. It considers a combination between the nominal stresses and the allowable stresses acting in different directions (see Equation (9)).

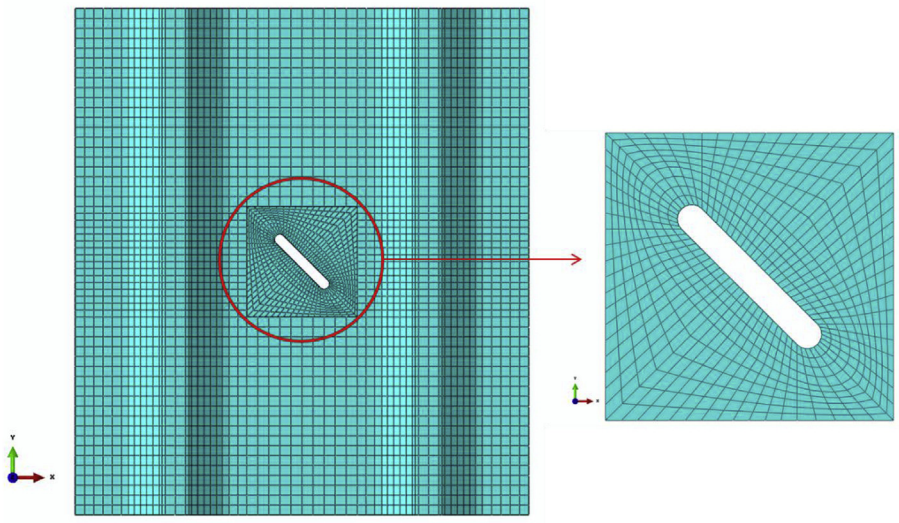

Fig. 4. FEM model.

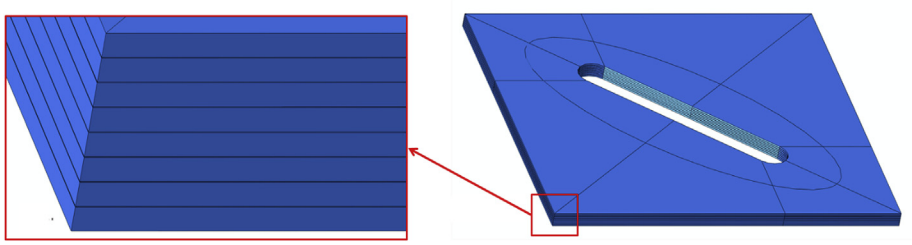

Fig. 6. Cohesive zone region.

Table 4
Cohesive elements stiffnesses.

Cohesive properties		Values
Elastic modulus	Mode I	1115000 MPa/mm
	Mode II	600000 MPa/mm
	Mode III	600000 MPa/mm
Strengths	Mode I	54 MPa
	Mode II	80 MPa
	Mode III	80 MPa

$$\left(\frac{\sigma_n}{N_{\max}}\right)^2 + \left(\frac{\sigma_t}{T_{\max}}\right)^2 + \left(\frac{\sigma_s}{S_{\max}}\right)^2 = 1 \tag{9}$$

Referring to Equation (9), N_{max} is the nominal stress in the pure normal mode, T_{max} is the nominal stress in the first shear direction and S_{max} is the nominal stress in the second shear direction.

The delamination growth under mixed-mode conditions is based on the energy dissipated during the damage process. This fracture energy is represented by the area under the traction-separation curve in Fig. 2 for each failure mode. The linear criterion, reported in Equation (10), has been adopted for the damage evolution phase:

$$\frac{G_I}{G_{IC}} + \frac{G_{II}}{G_{IIC}} + \frac{G_{III}}{G_{IIIC}} = 1 \tag{10}$$

where G_i is the Energy Release Rate and G_{ic} is the Critical Energy Release Rate associated to the fracture mode i [34]. As soon as equation (10) is satisfied, the mixed mode fracture energy G_c is evaluated according to the following relation:

$$G_C = \frac{1}{\left(\frac{G_I}{G_I+G_{II}+G_{III}}\cdot\frac{1}{G_{Ic}}\right) + \left(\frac{G_{II}}{G_I+G_{II}+G_{III}}\cdot\frac{1}{G_{IIc}}\right) + \left(\frac{G_{III}}{G_I+G_{II}+G_{III}}\cdot\frac{1}{G_{IIIc}}\right)} \tag{11}$$

Then the displacement $\delta_f = 2G_c/T_{eff}$ at complete failure (representative of the point C in Fig. 2) is evaluated where T_{eff} is the effective traction at damage initiation obtained from equation (9). Being δ_{max} the maximum attained displacement, the following relation is adopted in ABAQUS to compute the damage variable D for the degradation of the cohesive elements stiffness (Point B in Fig. 2),

$$D = \frac{\delta_f(\delta_{\max} - \delta_0)}{\delta_{\max}\left(\delta_f - \delta_0\right)} \tag{12}$$

3. Numerical analysis

In this section, the results from the performed numerical analyses, simulating the compressive behaviour of the investigated omega stiffened composite panel, are presented in detail. In the frame of the first numerical analysis only the intra-laminar damage onset and evolution have been taken into account by means of the aforementioned progressive failure model based on Hashin's failure criteria and continuum damage mechanics material degradation rules. In the frame of the second analysis, the inter-laminar damage has been considered too by adopted Cohesive Zone Model based elements. In the first subsection, the geometrical model is described together with the FEM characteristics, then, in the second

Table 5
Analysed models.

Model#1	Intra-laminar Damage
Model#2	Intra-laminar + Inter-laminar Damages

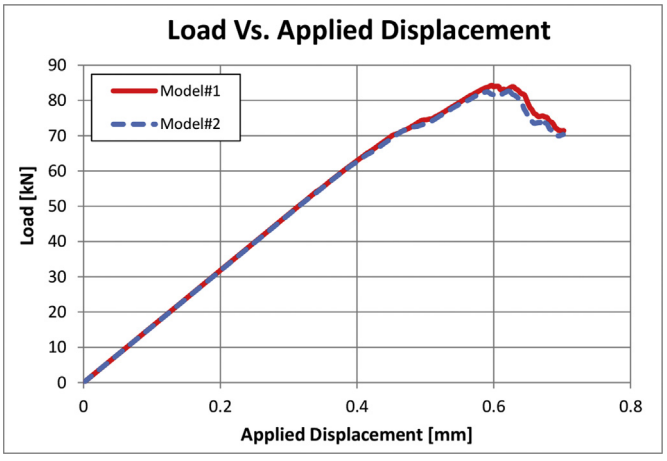

Fig. 7. Load vs. Applied Displacement curve.

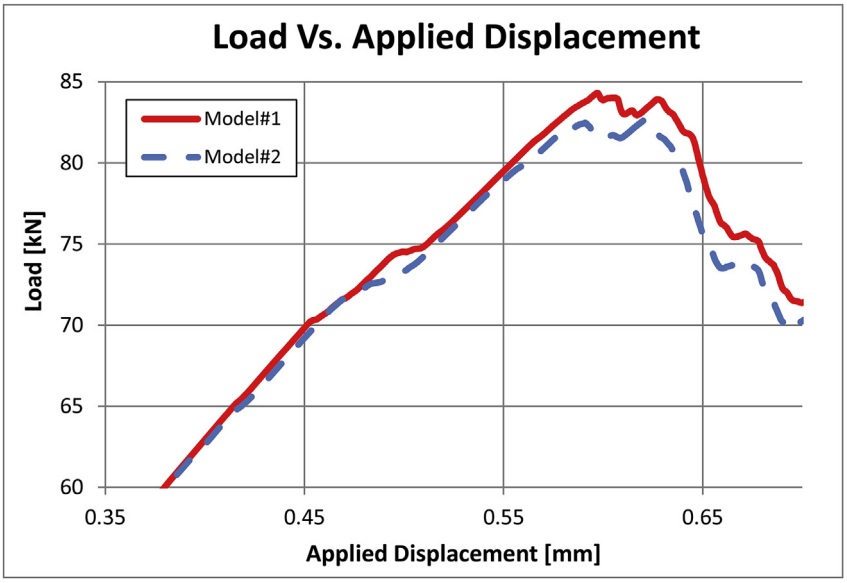

Fig. 8. Load vs. Applied Displacement curve – zoomed view.

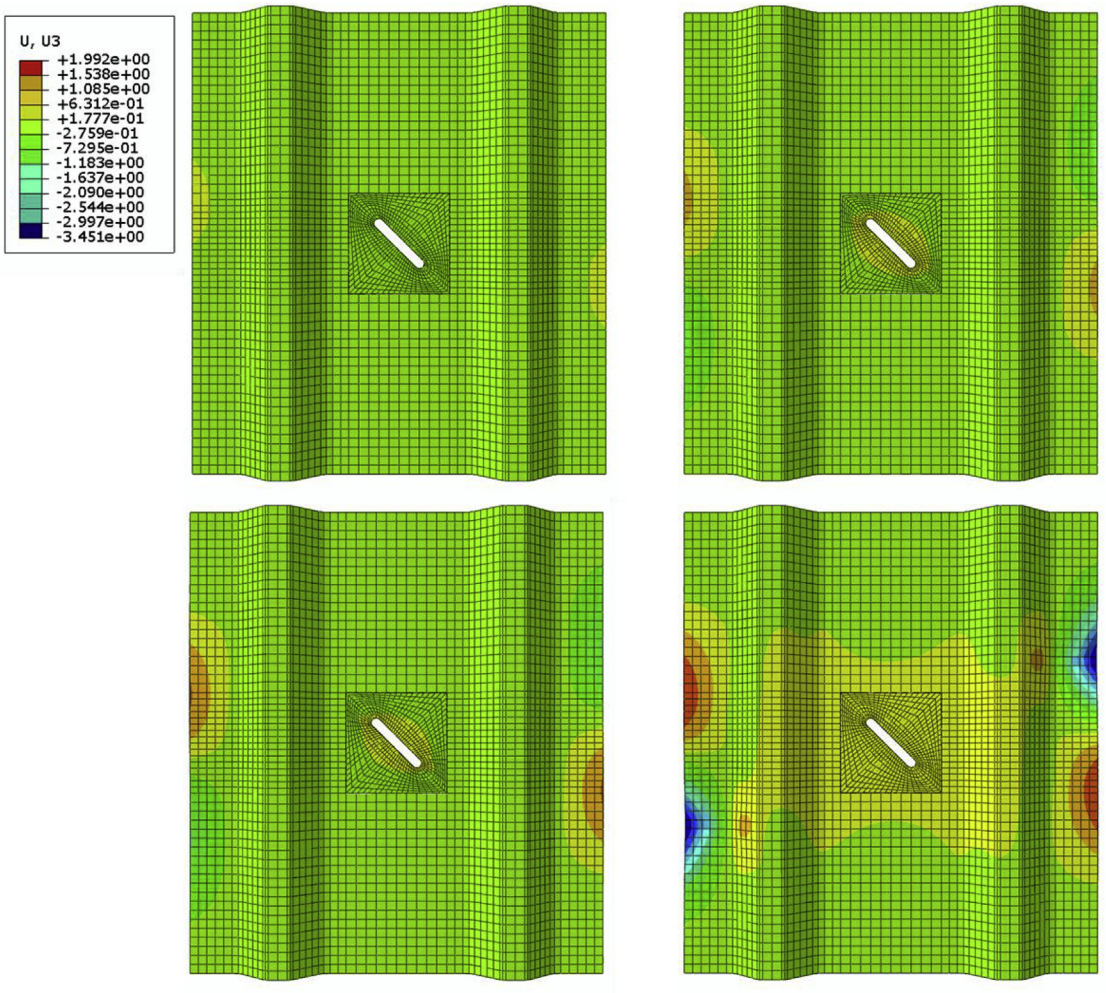

Fig. 9. Out-of-plane displacements at: (a) 0.4028 mm applied displacement (b) 0.478 mm applied displacement (c) 0.515 mm applied displacement (d) 0.701 mm applied displacement – Model#1.

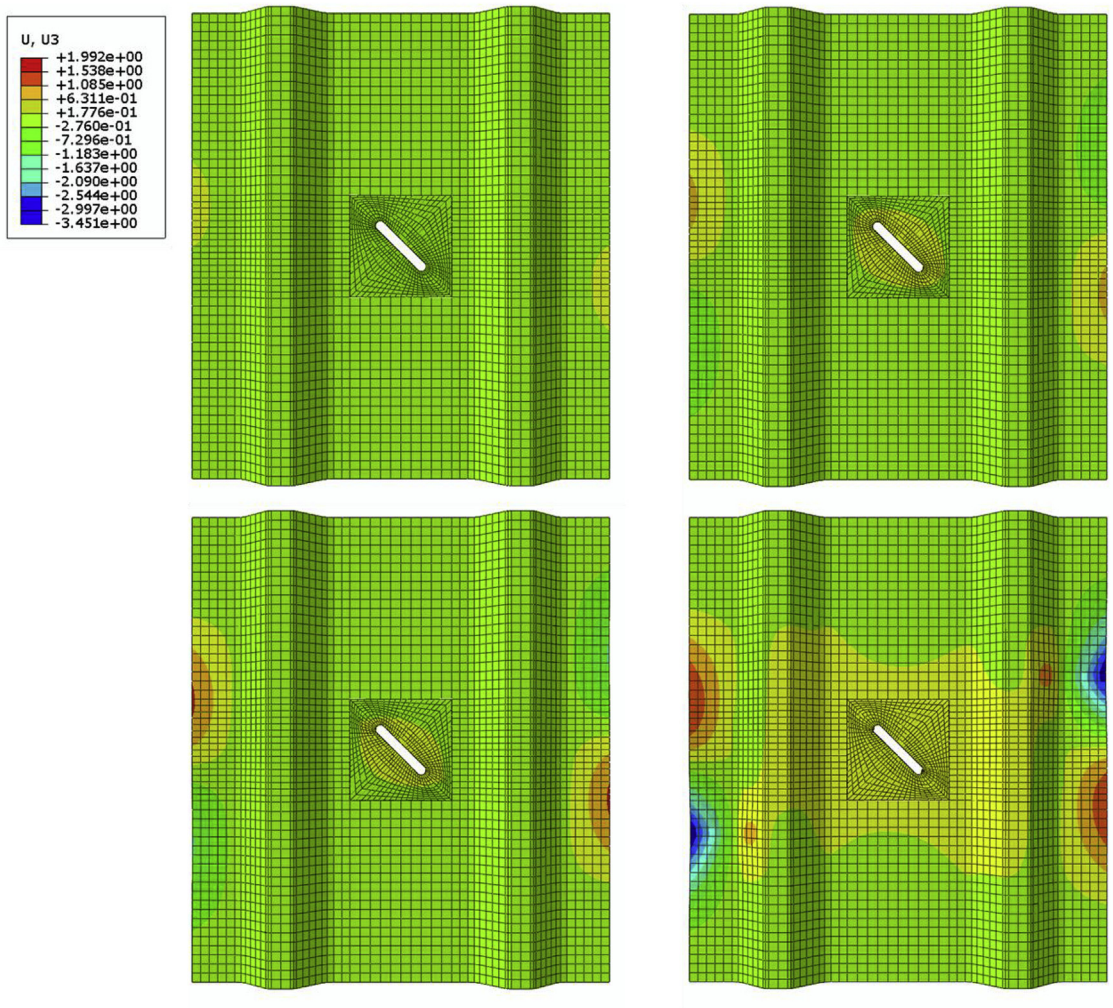

Fig. 10. Out-of-plane displacements at: (a) 0.4028 mm applied displacement (b) 0.477 mm applied displacement (c) 0.515 mm applied displacement (d) 0.701 mm applied displacement – Model#2.

subsection, the numerical results are presented and discussed.

3.1. Numerical test-case geometry and material description

The geometrical description of the omega stiffened panel and the properties of the adopted material system are, respectively, shown in Fig. 3 and Table 2. The intra-laminar strengths are listed in Table 3. The specimen has been manufactured by using two laminates, the first for the skin panel and the second for the omega stringers. The stacking sequence of both laminates is $\mathbf{[0\ 90]_s}$ with a ply thickness of 0.3 mm. The cut-out is located in the middle of the bay and oriented at 45° with respect to the loading direction. A global-local approach has been adopted to optimize the computational cost preserving, at the same time, the needed accuracy in the notch area. Indeed, two different regions have been considered within the introduced global-local approach: a coarser global region and a more refined local one (see Fig. 4).

The numerical model of the omega stiffened panel, shown in Fig. 4, has been realised by adopting the FEM code ABAQUS [34]. Both the global and local region, have been discretized with 8-node continuum shell elements SC8R and have been connected each other by means of TIE constraints (Multi Point Constraints).

According to Fig. 5, one edge of the panel has been clamped while a compressive displacement has been applied on the opposite one.

In the frame of the second analysis, as already mentioned, 8-node cohesive elements COH3D8 have been placed between the plies, in the local region. The mesh size dependency of cohesive elements is a known issue [35,36]. Indeed, it is possible to estimate the number of elements in a cohesive zone model to minimise the phenomenon in order to obtain accurate results [37]. In this work, each element of the ply has been connected to 4 cohesive elements. This discretization has been considered satisfactory in terms of accuracy of the results. The cohesive elements and the plies have been connected each other by means of TIE constraints (Multi Point Constraints). In Fig. 6, a detail of the local region of the panel highlighting the distribution of composite plies in the thickness direction and the cohesive layers is shown. In Table 4 the cohesive elements stiffnesses are reported.

The numerical models adopted to perform the analyses, whose results are presented and discussed in the next subsection, are summarized in Table 5 highlighting their main characteristics in

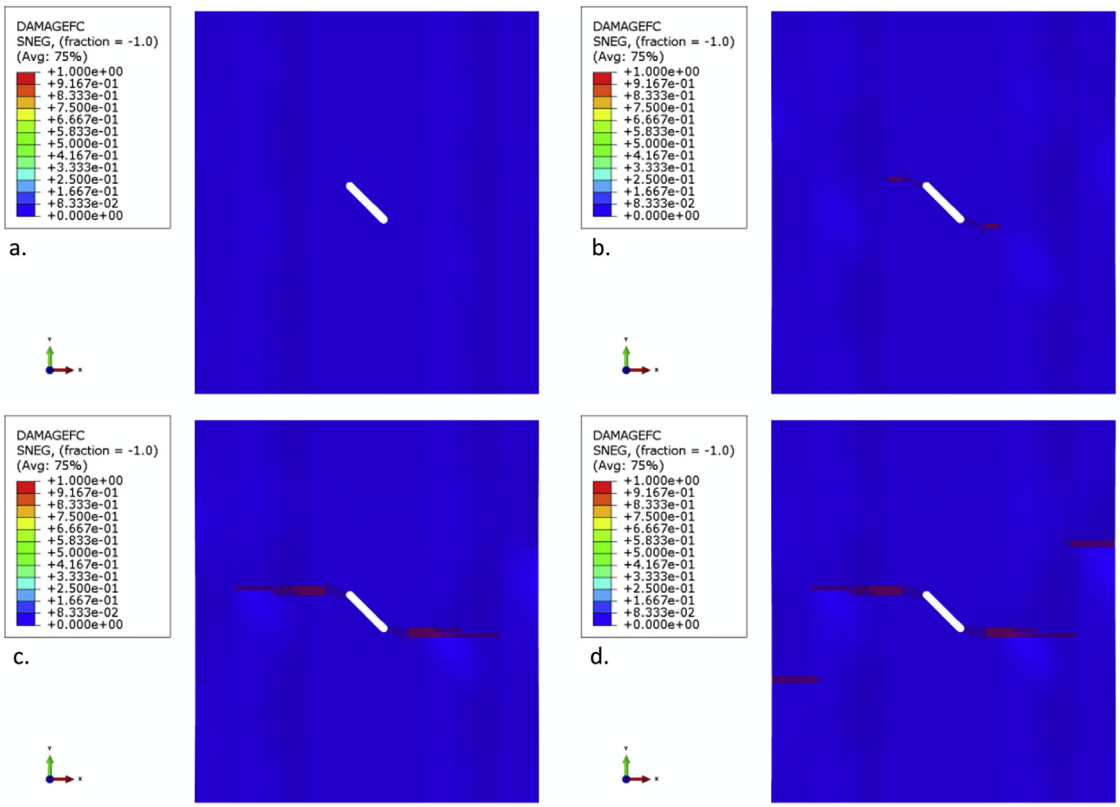

Fig. 11. Fibre compression failure at: (a) 0.4028 mm applied displacement (b) 0.6147 mm applied displacement (c) 0.6732 mm applied displacement (d) 0.701 mm applied displacement– Model#1.

terms of damage simulation capability.

3.2. Numerical results

The global compressive behaviour, in terms of load-displacement curves, for the investigated omega stiffened composite panel, obtained by adopting the two introduced numerical models is represented in Fig. 7. In this figure, the results obtained with the two numerical models are compared.

Looking at Fig. 7, the load-displacement curves, predicted by means of the two numerical models, seem to be almost coincident. However, providing a zoomed view of the final stage of compression, when damage mechanisms take place (see Fig. 8), interesting differences between the two models can be appreciated. Indeed, the two models provide the same output only up to 0.4 mm applied displacement. Beyond this point the predicted behaviour is different. Indeed, a slight loss of stiffness can be observed for the model#2 due to the onset of delamination at the edges of the notch.

The presence of delaminations seems to anticipate the progression of intra-laminar damage in terms of fibre breakage and the buckling phenomenon in the side bay of the panel (0.478 mm applied displacements for model#2 and 0.515 mm applied displacements for model#1). An anticipation of the global buckling and final failure phenomena can be also appreciated in the simulation performed with the model#2 with respect to the one performed with the model#1.

The deformed shapes with out-of-plane contour plots at different values of the applied displacements, are introduced in Fig. 9 and Fig. 10 respectively for the model#1 and model#2.

Indeed, the deformed shapes at (a) fibre breakage initiation (0.4028 mm applied displacement); (b) buckling in the side bays onset (0.478 mm applied displacement); (c) global buckling (0.515 mm applied displacement); (d) final damage growth state (0.701 mm applied displacement) are presented in these Figures.

The fibre compressive failure development at different values of the applied displacements, are introduced in Fig. 11 and Fig. 12 respectively for the model#1 and model#2.

According to Figs. 11 and 12, at 0.4028 mm applied displacement the fibre damage starts near the cut-out discontinuity and rapidly propagates perpendicular to the load direction up to the panel edges, causing the global collapse of the structure. Between 0.6 mm and 0.625 mm applied displacement, the fibre breakage reaches the stringer feet, passing from the local region to the global region and, subsequently, passing through the omega stringers.

A similar trend can be observed for matrix failure in Fig. 13 and Fig. 14 where, respectively, the matrix development at different values of the applied displacements, are introduced for the model#1 and the model#2.

From Fig. 15, introducing the fibre and matrix damage distribution along the thickness at the damage onset for model#1, it can be observed that, as expected, the intra-laminar damages modes distribution depends on the stacking sequence. 0° oriented plies are mostly affected by fibre failure while 90° oriented plies are mostly affected by matrix failure.

From the analysis performed by adopting Model#2, also the delamination onset and evolution can be observed. The delaminations distribution in the local region, which is the most

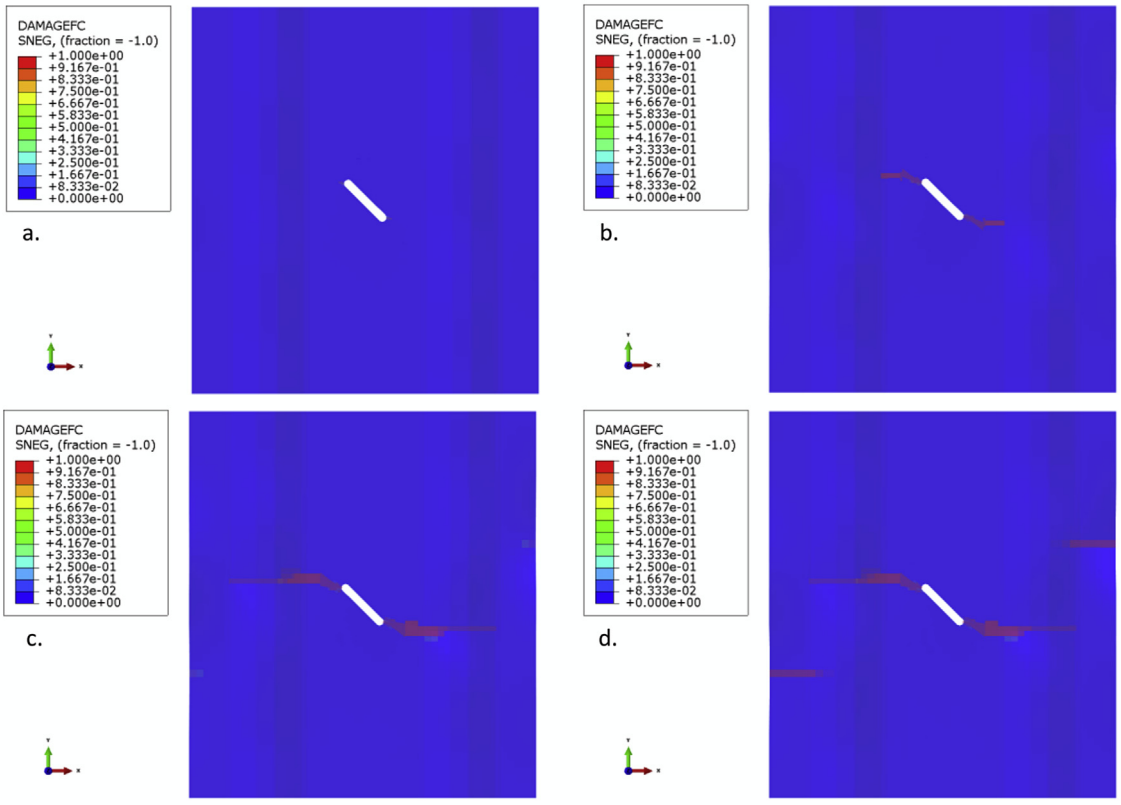

Fig. 12. Fibre compression failure at: (a) 0.4028 mm applied displacement (b) 0.6147 mm applied displacement (c) 0.6732 mm applied displacement (d) 0.701 mm applied displacement – Model#2.

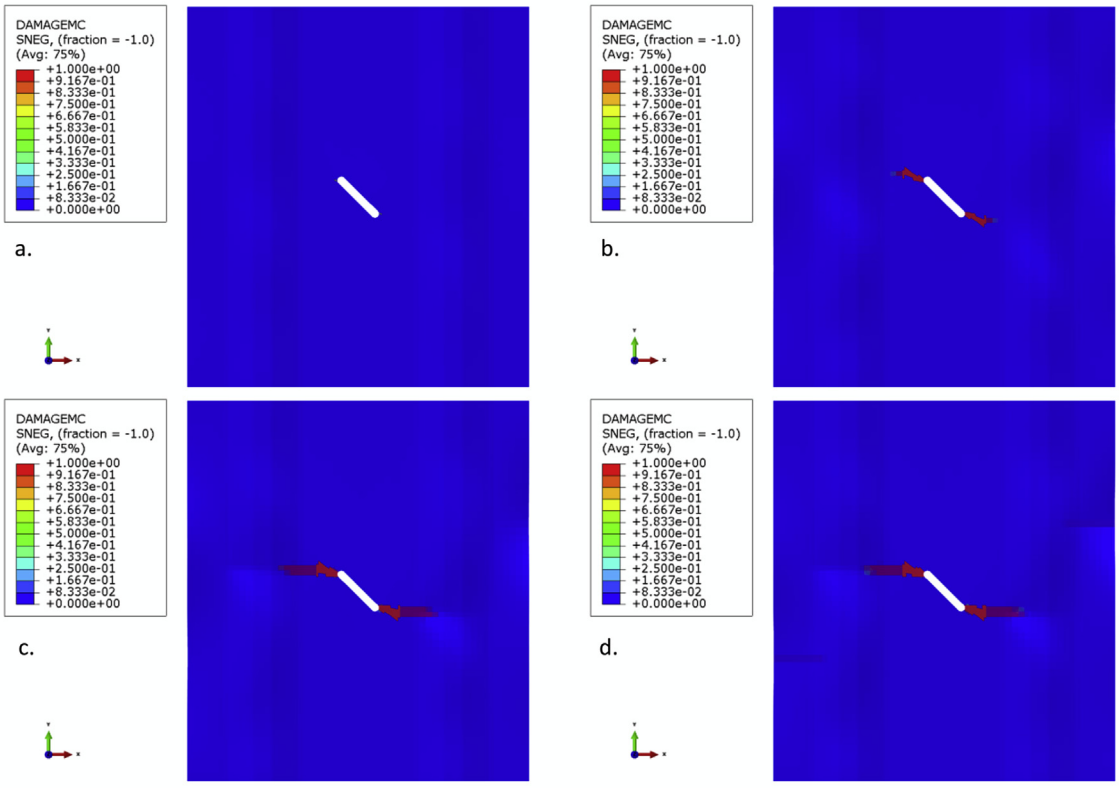

Fig. 13. Matrix compression failure at: (a) 0.4028 mm applied displacement (b) 0.6147 mm applied displacement (c) 0.6732 mm applied displacement (d) 0.701 mm applied displacement – Model#1.

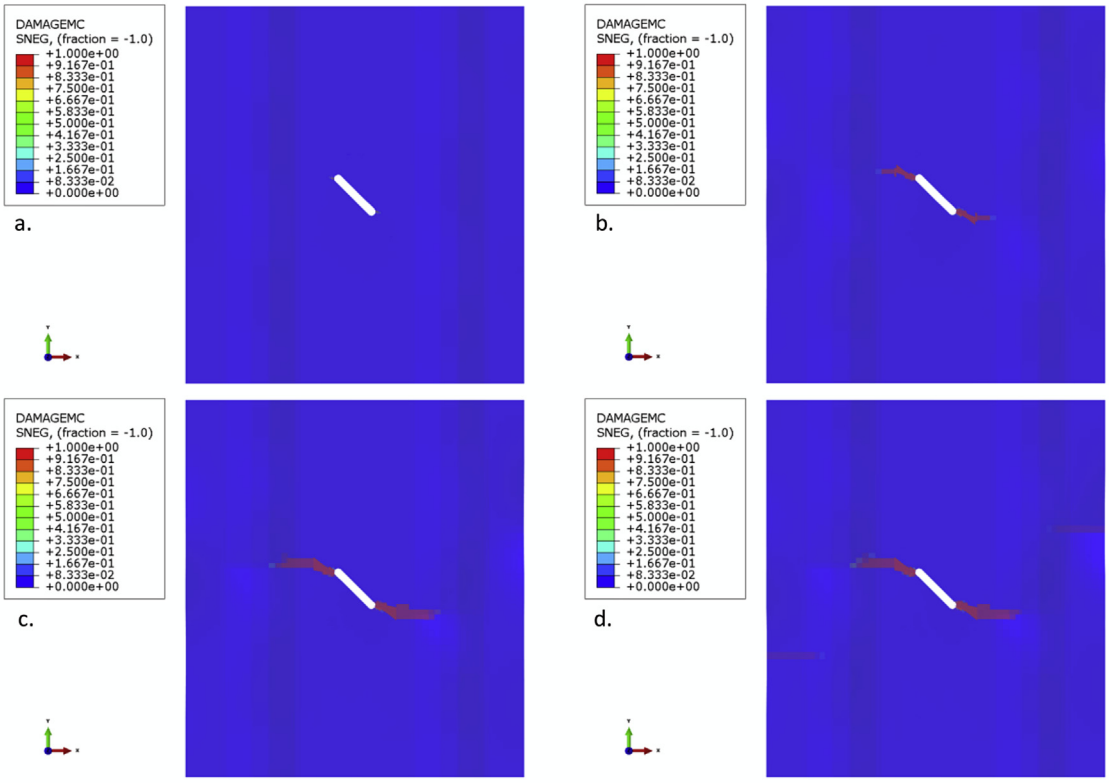

Fig. 14. Matrix compression failure at: (a) 0.4028 mm applied displacement (b) 0.6147 mm applied displacement (c) 0.6732 mm applied displacement (d) 0.701 mm applied displacement – Model#2.

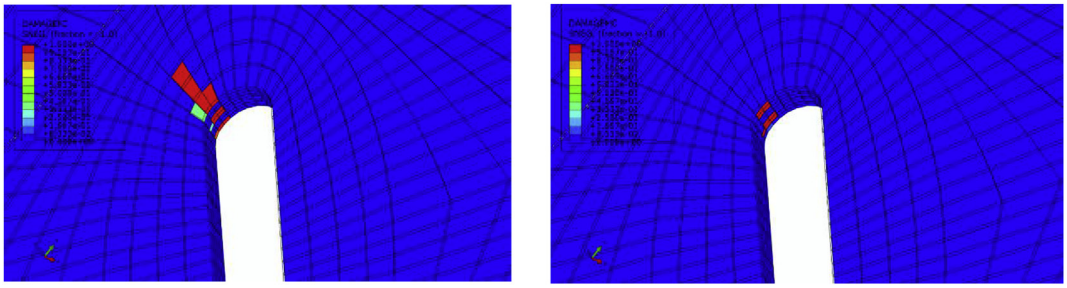

Fig. 15. a) Fibre compression failure and (b) Matrix compression failure at damage onset (0.4028 mm applied displacement).

affected by inter-laminar damages, is presented in Fig. 16 at different values of the applied displacements.

As it can be observed form Fig. 16, the inter-laminar damage onsets at the notch edge and propagated perpendicularly to the applied load direction. The largest delaminations are locate on the top and bottom interfaces. The internal interfaces show no appreciable delamination development.

As already remarked when commenting the load-displacement curve, the inter-laminar damage seems to start to develop significantly between 0.45 mm and 0.50 mm applied displacement causing the anticipation of the side bays buckling and fibre failure evolution.

During compression, at 0.701 mm applied displacement, the external delaminations buckle as shown in Fig. 17 where a zoomed view of the deformed shape at the notch edges is presented.

4. Conclusions

In this paper, the compressive behaviour of an omega stiffened panel with large notch damage has been investigated by performing numerical analyses. Numerical Models taking into account intra-lamina and inter-laminar damage evolution have been used for computations with the main purpose to investigate the influence of damage mechanisms interaction on the global compressive behaviour of the panel and on the damage development up to final failure.

The numerical analyses on the investigated composite stiffened panels have shown that the damage starts at the notch edges and

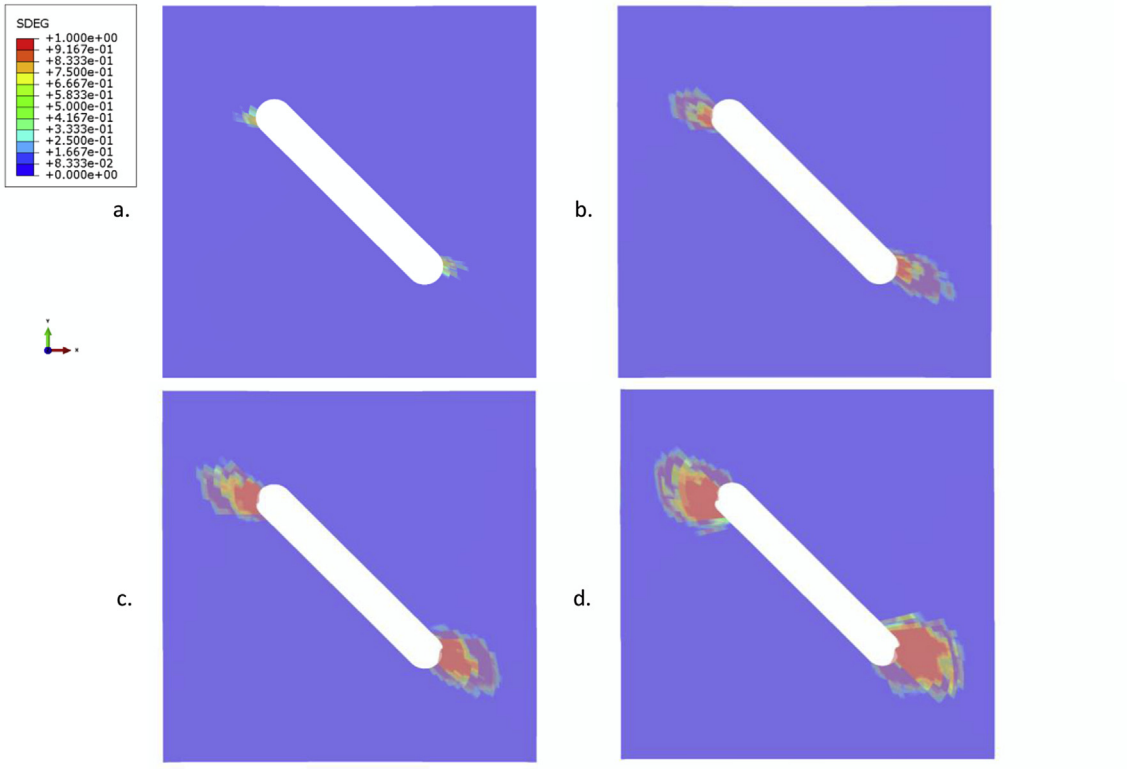

Fig. 16. Cohesive failure at: (a) 0.467 mm applied displacement (b) 0.547 mm applied displacement (c) 0.641 mm applied displacement (d) 0.701 mm applied displacement – Model#2.

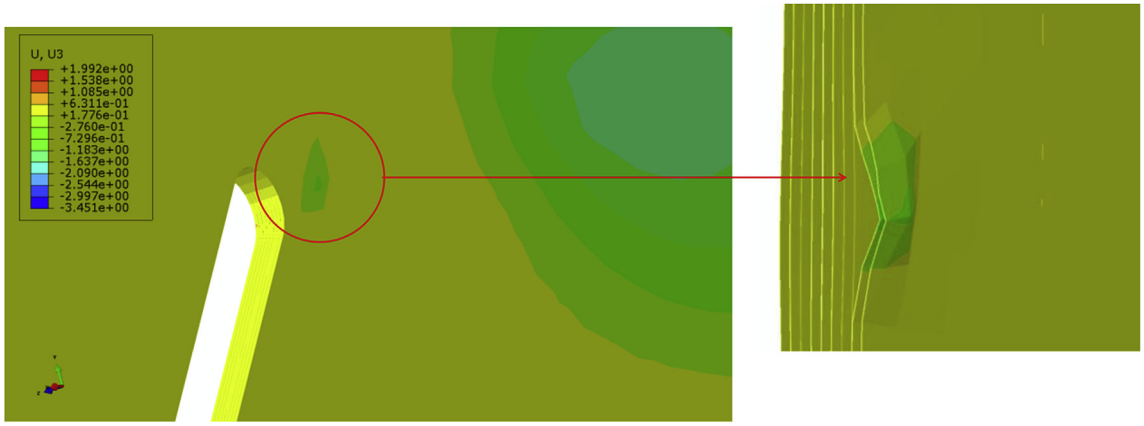

Fig. 17. Deformed shapes at: 0.701 mm applied displacement – zoomed view of the notch edges - Model#2.

propagates towards the panel edges perpendicularly with respect to the loading direction leading to a net tension failure mode. Compressive matrix and fibre failure mechanisms are predominant for the investigated panel. The damage distribution across the plies strongly depends, as expected, from the stacking sequence. Indeed, 0° plies are mostly affected by fibre damage, while 90° plies are mostly affected by the matrix damage.

The presence of inter-laminar damage in the notch area seems to anticipate the buckling phenomenon of the side bays of the panel and seems to accelerate the fibre failure propagation up to failure. Hence, the performed numerical analyses show that the use of an inter-laminar damage model, such as the cohesive zone model, combined with lamina degradation rules, is mandatory to correctly predict the damage evolution in a composite stiffened panel especially when the progression of a pre-existing damage is of main concern.

References

[1] Khdeir AA, Reddy JN. Buckling of cross-ply laminated beam with arbitrary boundary conditions. Compos Struct 1997;37(1):1–3.
[2] Kahya Volkan. Buckling analysis of laminated composite and sandwich beams by the finite element method. Compos Part B Eng 2016;91:126–34.

[3] Cricrì G, Perrella M, Calì C. Experimental and numerical post-buckling analysis of thin aluminium aeronautical panels under shear load. Strain 2014;50(3):208–22.
[4] Li ZM, Qiao P. Buckling and postbuckling behavior of shear deformable anisotropic laminated beams with initial geometric imperfections subjected to axial compression. Eng Struct 2015;85:277–92.
[5] Moradi S, Taheri F. Delamination buckling analysis of general laminated composite beams by differential quadrature method. Compos Part B Eng 1999;30:503–11.
[6] Caputo F, De Luca A, Sepe R. Numerical study of the structural behaviour of impacted composite laminates subjected to compression load. Compos Part B Eng 2015;79:456–65.
[7] Feng Y, Zhang H, Tan X, An T, He Y, Zheng J. Investigation on the buckling and postbuckling performance of aero stiffened composite panels under axial compression. Polym Compos 2016. IN PRESS, http://dx.doi.org/10.1002/pc.24239.
[8] Mo Yuming, Ge Dongyun, He Boling. Experiment and optimization of the hat-stringer-stiffened composite panels under axial compression. Compos Part B Eng 2016;84:285–93.
[9] Wanga XM, Cao W, Deng CH, Wang PY, Yue ZF. Experimental and numerical analysis for the post-buckling behavior of stiffened composite panels with impact damage. Compos Struct 2015;133:840–6.
[10] Su ZC, Tay TE, Ridha M. Progressive damage modeling of open-hole composite laminates under compression. Compos Struct 2015;122:507–17.
[11] Citarella R, Cricrì G. Three-dimensional BEM and FEM submodelling in a cracked FML full scale aeronautic panel. Appl Compos Mater 2014;21(3):557–77.
[12] Li Xiaole, Gao Weicheng, Liu Wei. Post-buckling progressive damage of CFRP laminates with a large-sized elliptical cutout subjected to shear loading. Compos Struct 2015;128:313–21.
[13] Sepe R, De Luca A, Lamanna G, Caputo F. Numerical and experimental investigation of residual strength of a LVI damaged CFRP omega stiffened panel with a cut-out. Compos Part B Eng 2016;102:38–56.
[14] Guob Shijun, Li Daochun, Zhang Xiang, Xiang Jinwu. Buckling and post-buckling of a composite C-section with cutout and flange reinforcement. Compos Part B Eng 2014;60:119–24.
[15] Ouinas Djamel, Achour Belkacem. Buckling analysis of laminated composite plates [(θ/−θ)] containing an elliptical notch. Compos Part B Eng 2013;55:575–9.
[16] Raimondo L, Iannucci L, Robinsona P. A progressive failure model for mesh-size independent FE analysis of composite laminates subject to low-velocity impact damage. Compo Sci Technol 2012;72:624–32.
[17] Tan SC. A progressive failure model for composite laminates containing openings. J Compos Mater 1991;25(5):556–77.
[18] Riccio A, Di Costanzo C, Di Gennaro P, Sellitto A, Raimondo A. Intra-laminar progressive failure analysis of composite laminates with a large notch damage. Eng Fail Anal 2017;73:97–112.
[19] Bai Yujie, Zhang Xiao-Zhang. Progressive failure analysis of open-hole composite hoops under radial loading. Compos Part B Eng 2016;97:336–43.
[20] Namdar Ö, Darendeliler H. Buckling, postbuckling and progressive failure analyses of composite laminated plates under compressive loading. Compos Part B Eng 2017;120:143–51.
[21] Tarfaoui M, El Moumen A, Lafdi K. Progressive damage modeling in carbon fibers/carbon nanotubes reinforced polymer composites. Compos Part B Eng 2017;112:185–95.
[22] Treutenaere S, Lauro F, Bennani B, Matsumoto T, Mottola E. Modelling of the intralaminar matrix damage with friction effects of fabric reinforced polymers. Compos Part B Eng 2017;111:60–73.
[23] Fernández-Cañadas LM, Iváñez I, Sanchez-Saez S. Influence of the cohesive law shape on the composite adhesively-bonded patch repair behaviour. Compos Part B Eng 2016;91:414–21.
[24] Reinoso J, Paggi M, Blázquez A. A nonlinear finite thickness cohesive interface element for modeling delamination in fibre-reinforced composite laminates. Compos. Part B: Eng. 2017;109:116–28.
[25] Liu Guangyan, Bao Hongchen, Tang Kaili. Damage prediction in notched fiber-reinforced composite laminates. Compos Interfaces 2017;24(3):279–90.
[26] Chang Fu-Kuo, Chang Kuo-Yen. A progressive damage model for laminated composites containing stress concentrations. J Compos Mater 1987;21(9):834–55.
[27] Soto A, González EV, Maimí P, Turon A, Sainz de Aja JR, de la Escalera FM. Cohesive zone length of orthotropic materials undergoing delamination. Eng Fract Mech 2016;159:174–88.
[28] Amiri-Rad A, Mashayekhi M, van der Meer FP. Cohesive zone and level set method for simulation of high cycle fatigue delamination in composite materials. Compos Struct 2017;160:61–9.
[29] Reinoso J, Paggi M, Blázquez A. A nonlinear finite thickness cohesive interface element for modeling delamination in fibre-reinforced composite laminates. Compos. Part B: Eng. 2017;109:116–28.
[30] Giuliese G, Palazzetti R, Moroni F, Zucchelli A, Pirondi A. Cohesive zone modelling of delamination response of a composite laminate with interleaved nylon 6,6 nanofibres. Compos Part B Eng 2015;78:384–92.
[31] Bergan A, Dávila C, Leone F, Awerbuch J, Tan T. A Mode I cohesive law characterization procedure for through-the-thickness crack propagation in composite laminates. Compos Part B Eng 2016;94:338–49.
[32] Camanho PP, Davila CG, Moura MF. Numerical simulation of mixed-mode progressive delamination in composite materials. J Compos Mater 2003;37(16):1415–38.
[33] Lepore MA, Perrella M. From test data to FE code: a straightforward strategy for modelling the structural bonding interface. In: Frattura, editor. Integrità strutturale, vol. 39; 2017. p. 191–201.
[34] ABAQUS analysis User's manual 6.11. 2011.
[35] Turon A, Dávila CG, Camanho PP, Costa J. An engineering solution for mesh size effects in the simulation of delamination using cohesive zone models. Eng Fract Mech 2007;74:1665–82.
[36] Turon A, Camanho PP, Costa J, Renart J. Accurate simulation of delamination growth under mixed-mode loading using cohesive elements: definition of interlaminar strengths and elastic stiffness. Compos Struct 2010;92:1857–64.
[37] Davila CG, Camanho PP, De Moura MF. Mixed-Mode Decohesion Elements for Analyses of Progressive Delamination in Proceedings of the 42nd AIAA/ASME/ASCE/AHS/ASC Structures, Structural Dynamics and Materials Conference, Seattle, Washington, 2001.